AIMS Biophysics

AIMS Biophysics, 13(4): 482−500.
DOI: 10.3934/biophy.2026024
Received: 15 July 2026
Revised: 14 September 2026
Accepted: 22 October 2026
Published: 02 November 2026

http://www.aimspress.com/journal/biophysics

Research article

An ODE model of LPS-induced neuroinflammation with bistability and dose-dependent switching

Ekaterina Kukushkina[1,2,*], Elena Lebedeva[1], Dmitry Traktirov[2] and Marina Karpenko[1,2]

[1] Peter the Great St. Petersburg Polytechnic University, St. Petersburg, Russia
[2] Institute of Experimental Medicine, St. Petersburg, Russia

* **Correspondence:** Email: eskukushkina7@gmail.com; Tel: +79216499157.

Abstract: Systemic administration of lipopolysaccharide (LPS) is widely used to model neuroinflammation, yet it remains unclear how a transient systemic inflammatory challenge can lead either to resolution or to sustained central inflammatory activity. We developed a phenomenological ordinary differential equation (ODE) model of LPS-induced neuroinflammation in rodents comprising four dynamic variables: the systemic LPS signal, central proinflammatory cytokine activity, microglial activation, and the severity of inflammation-associated neuronal and tissue alterations. Peripheral cytokine signaling and blood–brain barrier-mediated communication were not represented as separate state variables; instead, their combined initiating effect was coarse-grained into a transient LPS-dependent input to the central cytokine response. Importantly, all model parameters were fixed, and the LPS dose entered the model solely through the initial condition. Analysis of equilibria, local stability, bifurcations, and basins of attraction showed that with sufficiently strong damage-dependent feedback, the system exhibits bistability between a stable resolution state and a stable persistent neuroinflammatory state, with an intermediate saddle equilibrium coexisting with them. For the reference parameter set, two positive equilibria (i.e., a saddle and a stable persistent state) emerged through a saddle-node bifurcation at the critical damage-dependent feedback coefficient $\rho_c = 1.476$. The switching threshold between resolving and persistent outcomes was $D_c \approx 0.86$ mg/kg LPS. Near this threshold, trajectories exhibited markedly prolonged transients before resolution, whereas suprathreshold doses converged to the persistent attractor. Under global parameter variation, bistability was preserved in 94.9% of the parameter sets examined, and a separate analysis of the Hill coefficient showed that bistability persisted over $n = 1.6$–2.4, although the numerical dose threshold shifted substantially. Thus, dose-dependent outcomes arise from the intrinsic nonlinear dynamics of a fixed-parameter ODE system. The model provides a dynamical-systems framework for interpreting

resolution, prolonged near-threshold responses, and persistent neuroinflammatory states following a transient systemic LPS challenge.

Keywords: LPS; neuroinflammation; microglia; ordinary differential equations; bistability; saddle-node bifurcation; dynamical systems

Abbreviations: LPS: lipopolysaccharide; ODE: ordinary differential equation; CNS: central nervous system; BBB: blood-brain barrier; TNF-α: tumor necrosis factor α; IL: interleukin; NF-κB: nuclear factor κB

1. Introduction

Systemic administration of lipopolysaccharide (LPS) is widely used to model neuroinflammation because LPS induces a pronounced peripheral inflammatory response and can activate central immune mechanisms, including increased levels of proinflammatory cytokines in the brain and microglial activation. Experimental studies have shown that systemic LPS exposure induces both peripheral and central inflammation; systemic LPS administration has also been associated with microglial activation and increased expression of proinflammatory factors in the brain, including TNF-α, MCP-1, IL-1β, and NF-κB [1,2].

One approach to formalizing inflammatory processes is to construct mathematical models based on ordinary differential equations (ODEs). ODE models can describe nonlinear feedback, threshold effects, stable states, and transitions between resolving and persistent inflammatory regimes. Reynolds et al. developed a model of the acute inflammatory response based on nonlinear interactions among key components of inflammation [3]. However, that model describes the regulation of systemic inflammation rather than a central microglia–cytokine–damage feedback loop capable of sustaining neuroinflammation after a transient systemic challenge. A model more closely related to neuroinflammation was proposed by Vaughan et al., whose ODE system links cytokine regulation, microglial activation, and CNS tissue damage following traumatic brain injury [4]. This model provides an important example of coupling inflammatory signaling to tissue damage, but it was developed for traumatic brain injury rather than systemic LPS exposure.

In the present study, we formulate an ODE model focused on central neuroinflammatory dynamics initiated by a transient systemic LPS challenge. Rather than explicitly representing the kinetics of peripheral cytokines and blood–brain barrier permeability, the model coarse-grains their combined contribution into an effective transient LPS-dependent input to the central cytokine response. The central circuit contains reciprocal interactions among microglial activation, proinflammatory cytokine activity, and neuronal alterations. The main question is whether a fixed-parameter ODE model can generate qualitatively distinct long-term outcomes solely as a consequence of differences in the magnitude of the initial LPS challenge. We therefore analyze equilibria, local stability, the saddle-node bifurcation, dose-dependent outcomes associated with different basins of attraction, and parameter sensitivity. Beyond the specific LPS paradigm, a dynamical-systems formulation of this kind makes it possible to distinguish interventions that reduce the magnitude of the acute response from interventions that modify the architecture of the central feedback circuit itself. This distinction is relevant to the design of preclinical studies because the model suggests that the two classes of

intervention may differ qualitatively, rather than merely quantitatively, in their long-term outcomes.

The aim of the present study was to determine whether nonlinear feedback within a minimal central neuroinflammatory circuit can support the coexistence of resolving and persistent states and thereby generate a dose-dependent transition following a single systemic LPS challenge.

2. Materials and methods

2.1. Model scope and variables

The model was formulated from the outset as an ODE system. Four dynamic variables were considered: L(t), the systemic LPS signal; C(t), the level of proinflammatory cytokine activity in the brain; M(t), the level of microglial activation; and D(t), the severity of inflammation-associated neuronal and tissue alterations. All variables were nonnegative. M(t) was additionally bounded by a nominal maximum Mmax. Microglia were represented as a finite pool of activatable central immune cells, consistent with the bounded formulation used here [5,6].

The model was intentionally focused on a central dynamic circuit capable of sustaining neuroinflammation after the initiating systemic stimulus had disappeared. Information about systemic inflammation may reach the CNS through circulating mediators, endothelial and BBB-associated signaling, and other routes of communication between the periphery and the CNS [7–10]. These processes were not represented as separate state variables. Instead, their combined initiating effect on the CNS was coarse-grained into the transient function σL(L), which should be interpreted as an effective transduced systemic inflammatory input rather than as direct entry of circulating LPS into brain tissue. This modeling choice reduces peripheral-to-CNS signal transmission to a phenomenological input and is explicitly acknowledged as a limitation of the model.

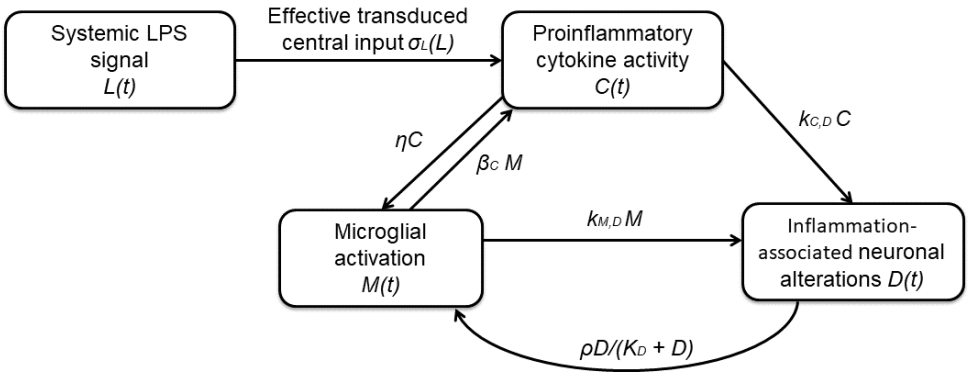


Figure 1. Model structure. Systemic LPS generates a transient effective input to central cytokine activity. The central feedback circuit includes microglia-dependent cytokine production, cytokine- and microglia-dependent formation of neuronal and tissue alterations, and $D(t)$-dependent enhancement of microglial activation. Processes involving peripheral cytokines and the BBB are coarse-grained into $\sigma_L(L)$ and are not represented as explicit dynamic variables. For clarity, the linear elimination, deactivation, and resolution terms $-\delta_L L$, $-\delta_C C$, $-k_{\text{out}} M$, and $-k_{D,\text{out}} D$ are not shown in the diagram. Each activating interaction shown in the diagram corresponds directly to a term in Eqs. (1)–(7).

2.2. Model formulation

The model is defined by the following system:

$$\begin{cases} \dfrac{\mathrm{d}L}{\mathrm{d}t} = -\delta_L L, \qquad L(0) = D_{\mathrm{LPS}} & (1) \\ \dfrac{\mathrm{d}C}{\mathrm{d}t} = \beta_C M + \sigma_L(L) - \delta_C C & (2) \\ \dfrac{\mathrm{d}M}{\mathrm{d}t} = k_{\mathrm{in}} H(S)(M_{\max} - M) - k_{\mathrm{out}} M & (3) \\ \dfrac{\mathrm{d}D}{\mathrm{d}t} = k_{C,D} C + k_{M,D} M - k_{D,\mathrm{out}} D & (4) \end{cases}$$

The saturating systemic input is defined as

$$\sigma_L(L) = \sigma_{\max} \frac{L^m}{K_L{}^m + L^m} \tag{5}$$

and the total stimulus governing microglial activation is

$$S = \eta C + \rho \frac{D}{K_D + D} \tag{6}$$

Microglial activation is described by the Hill function

$$H(S) = \frac{S^n}{K_M{}^n + S^n} \tag{7}$$

Equation (1) describes an exponentially decaying systemic LPS-related signal following a single administration. The LPS dose enters the model only through the initial condition L(0) = DLPS; no kinetic or feedback parameter varies with dose. Equation (2) describes central proinflammatory cytokine activity. The term σL(L) represents a transient CNS-directed inflammatory input induced by systemic LPS exposure, βC M represents cytokine production associated with activated microglia, and δC C represents clearance/resolution of the cytokine response. The saturating form of σL(L) is a phenomenological modeling choice used to represent a bounded nonlinear systemic input and is not intended to describe receptor-level kinetics. LPS signaling is mediated through TLR4-associated pathways [11]. Systemic LPS challenge following intraperitoneal administration has also been shown to induce inflammatory changes in rat dorsal root ganglia [12].

Equation (3) describes microglial activation. The activating signal S combines cytokine-dependent stimulation (ηC) and a saturating damage-dependent feedback term ρD/(KD + D). Activated microglia are a major source of inflammatory mediators [5], and reciprocal interactions between activated microglia and damaged neural tissue have been implicated in the persistence of neuroinflammatory and neurodegenerative processes [13–15]. The factor (Mmax − M) imposes an upper bound on activation, whereas kout M represents deactivation.

The Hill coefficient n = 2 was selected as a reference phenomenological value producing threshold-like microglial activation. The condition n > 1 is important for the subsequent analysis: only

for $n > 1$ is $H'(0) = 0$, so that the resolution state E0 remains locally asymptotically stable for all admissible parameter values and the nonzero states can emerge only as a pair through a saddle-node bifurcation. At $n = 1$, $H'(0) = 1/KM$ is nonzero and the stability of E0 becomes parameter-dependent. For the reference parameter set, E0 is unstable at $n = 1$ and the bistable structure analyzed below does not arise. The specific value $n = 2$ was adopted as the reference value, and its influence was evaluated separately (Section 2.6).

Equation (4) describes the severity of inflammation-associated neuronal and tissue alterations generated by central cytokine activity and activated microglia; the term kD,outD represents resolution, compensation, or removal of reversible damage-associated alterations. This variable is intended as an aggregate representation of inflammatory tissue stress and associated damage-related alterations rather than as a direct measure of irreversibly lost neurons; LPS-associated neuronal and synaptic alterations have been demonstrated experimentally [16,17].

For nonnegative initial conditions, the nonnegative orthant is positively invariant. At $L = 0$, $dL/dt = 0$; at $C = 0$ and $D = 0$, the corresponding derivatives are nonnegative; and at $M = 0$, $dM/dt \geq 0$. At $M = Mmax$, the activation term vanishes and $dM/dt = -koutMmax < 0$, so $M(t)$ remains bounded within $[0, Mmax]$.

2.3. Parameterization and representation of dose

Parameter values were treated as a computationally calibrated, biologically plausible reference set rather than as universal biological constants, consistent with the use of phenomenological dynamical models of inflammatory and neuroimmune processes [3,18]. The parameter set is given in Table 1. The reference parameterization was selected to reproduce a biologically plausible dynamical regime with threshold-like microglial activation, direct cytokine- and microglia-dependent contributions to $D(t)$, and damage-dependent amplification of microglial activation. Because responses to LPS depend on species, strain, route of administration, age, sex, and baseline immune status [19], the parameter set was intended to represent a reference dynamical regime rather than a universal dose–response law.

The reference value $\rho = 2.30$ was selected within the qualitative calibration so that a single 1 mg/kg LPS challenge lies on the persistent side of the model switching threshold, consistent with published evidence of prolonged central inflammatory alterations following a single systemic 1 mg/kg LPS challenge in rodents [20]. Consequently, the numerical critical dose reported below is a calibrated model quantity rather than an independently predicted universal biological threshold. The parameter m determines the steepness of the effective transduced input $\sigma_L(L)$ as a function of the systemic LPS level, whereas K_L is its half-saturation level. The value $m = 2$ was adopted as a smooth saturating representation of an acute systemic challenge in which differences among the investigated doses remain encoded in the magnitude of the initial perturbation. At $m = 1$, the dose dependence becomes excessively shallow, whereas at larger values of m, $\sigma_L(L)$ approaches a step-like function and doses above the half-saturation level become progressively less distinguishable in terms of input magnitude.

Table 1. Reference parameter set for the fixed-parameter model.

Parameter	Value	Units	Biological interpretation
δ_L	1.00	day^{-1}	Decay rate of the systemic LPS-related signal
β_C	0.45	day^{-1}	Microglia-dependent production of central cytokine activity
δ_C	0.80	day^{-1}	Clearance/resolution rate of central cytokine activity
k_{in}	0.90	day^{-1}	Maximum rate of microglial activation
k_{out}	0.38	day^{-1}	Rate of microglial deactivation
η	0.55	—	Relative contribution of cytokine activity to microglial stimulation
K_M	0.90	a.u.	Half-saturation constant of the total microglial stimulus
M_{max}	1.00	a.u.	Nominal maximum level of microglial activation
ρ	2.30	a.u.	Strength of damage-dependent feedback from tissue alterations to microglia
K_D	0.60	a.u.	Half-saturation constant of damage-dependent activation
$k_{C,D}$	0.008	day^{-1}	Cytokine-dependent contribution to neuronal and tissue alterations
$k_{M,D}$	0.030	day^{-1}	Microglia-dependent contribution to neuronal and tissue alterations
$k_{D,\text{out}}$	0.060	day^{-1}	Rate of resolution/compensation of neuronal and tissue alterations
σ_{max}	1.00	a.u. day^{-1}	Maximum effective transduced systemic inflammatory input
K_L	0.20	mg/kg	Half-saturation level of the LPS-dependent input
m	2	—	Hill coefficient for the acute LPS-dependent input
n	2	—	Hill coefficient for threshold-like microglial activation

2.4. Equilibria, stability, and bifurcation analysis

Equilibria were determined by setting Eqs. (1)–(4) equal to zero. For any single LPS challenge, $L^* = 0$ and therefore $\sigma_L(L^*) = 0$. The equilibrium relations for C and D can then be expressed explicitly in terms of M^*:

$$C^* = \frac{\beta_C}{\delta_C} M^* = aM^* \tag{8}$$

$$D^* = \frac{k_{C,D}\frac{\beta_C}{\delta_C} + k_{M,D}}{k_{D,\text{out}}} M^* = bM^* \tag{9}$$

For the reference parameter set, $a = 0.5625$ and $b = 0.5750$. Substitution into Eqs. (3), (6), and (7)

yields the scalar equilibrium equation

$$F(M^*) = k_{\text{in}}H(S(M^*))(M_{\max} - M^*) - k_{\text{out}}M^* = 0 \tag{10}$$

$$S(M^*) = \eta a M^* + \rho \frac{bM^*}{K_D + bM^*} \tag{11}$$

The resolution equilibrium $E_0 = (L^*, C^*, M^*, D^*) = (0,0,0,0)$ exists for all parameter values. For $n > 1$, $H'(0) = 0$. Consequently, the eigenvalues of the Jacobian at E_0 reduce to $-\delta_L$, $-\delta_C$, $-k_{\text{out}}$, and $-k_{D,\text{out}}$; because all corresponding parameters are positive, all four eigenvalues are negative, and E_0 is therefore locally asymptotically stable throughout the considered admissible parameter domain. Positive equilibria were determined numerically from Eq. (10), and their local stability was assessed from the eigenvalues of the full four-dimensional Jacobian.

A one-parameter bifurcation analysis was performed with respect to ρ, the damage-dependent feedback coefficient. Equilibrium branches were tracked numerically by solving Eq. (10) as ρ was varied sequentially. The saddle-node bifurcation point was identified from the simultaneous conditions $F(M^*) = 0$ and $\partial F/\partial M^* = 0$. This analysis determines the value of ρ at which two positive equilibria — a saddle and a stable persistent state — emerge while the resolution state E_0 remains stable.

2.5. Dose-dependent basin switching and the critical LPS dose

Numerical simulations were performed following a single systemic challenge with $L(0) = D_{\text{LPS}}$ and $C(0) = M(0) = D(0) = 0$. Because all model parameters were fixed, varying D_{LPS} changed only the magnitude of the transient initial perturbation. Under bistability, the stable manifold of the saddle separates the basin of attraction of E_0 from that of the nonzero persistent state. The critical dose D_c was defined as the value of $L(0)$ at which the one-dimensional line of initial conditions ($L(0)$, 0, 0, 0) intersects the basin boundary: for $D_{\text{LPS}} < D_c$, the corresponding initial condition belongs to the basin of E_0, whereas for $D_{\text{LPS}} > D_c$ it belongs to the basin of E_2. D_c was estimated by bisection in $L(0)$, with trajectories integrated for up to 500 days to classify their long-term outcome. All systems were integrated using the LSODA solver (scipy.integrate.solve_ivp) with relative tolerance rtol = 1×10^{-9} and absolute tolerance atol = 1×10^{-11}. Equilibria were located on a uniform grid of 5000 points in M over the interval (0, $M_{\max}$), followed by root refinement with Brent's method; the Jacobian was evaluated numerically using central differences with a step size of 1×10^{-6}. The saddle-node bifurcation point was determined by numerically solving $F(M^*) = 0$ and $\partial F/\partial M^* = 0$ simultaneously. A trajectory was classified as persistent if M at day 500 exceeded the arithmetic mean of the saddle and persistent equilibrium values of M; bisection in $L(0)$ was performed for up to 60 iterations or until the interval width reached 1×10^{-5} mg/kg.

Time courses were calculated over 0–100 days for representative doses below, near, and above the switching threshold (0.3, 0.8, 1.0, and 5.0 mg/kg). Longer integration to 500 days was used only to obtain unambiguous attractor classification near the basin boundary.

2.6. Global parameter sensitivity and structural sensitivity to n

Robustness to parameter uncertainty was assessed using Latin hypercube sampling with 1000

parameter sets and a fixed random seed of 9. Fourteen rate, coupling, and half-saturation parameters (δ_L, β_C, δ_C, k_{in}, k_{out}, η, K_M, ρ, K_D, $k_{C,D}$, $k_{M,D}$, $k_{D,out}$, σ_{max}, and K_L) were varied independently and simultaneously within ± 20% of their reference values. $M_{max} = 1$ was kept fixed as a normalization of the scale of M and was therefore not treated as an independent sensitivity parameter. The exponents m and n were also held fixed in this analysis.

For each parameter set, we evaluated the presence or absence of bistability, the critical dose D_c, and the microglial activation level M^* at the persistent equilibrium. For bistable parameter sets, the numerical search for D_c was extended up to 80 mg/kg; D_c was considered undefined within the investigated range when an LPS-only initial condition did not lead to the persistent outcome at doses up to 80 mg/kg. Partial rank correlation coefficients (PRCCs) were calculated only for parameter sets with a defined D_c and were used to quantify monotonic associations between the varied parameters and D_c while controlling for the remaining varied parameters. To accelerate the calculations in this analysis, trajectories were integrated to 400 days using rtol = 2×10^{-6} and atol = 1×10^{-8}, equilibria were searched on a 900-point grid, and bisection in $L(0)$ was limited to 15 iterations.

The input-function exponent $m = 2$ was retained as a structural assumption determining the shape of the transient systemic input; sensitivity of D_c to variation in m was not evaluated separately. Because n changes the shape of the activation nonlinearity rather than merely rescaling a rate or coupling parameter, its influence was examined separately rather than included in the global parameter uncertainty analysis. The analysis was repeated for n = 1.6, 1.8, 2.0, 2.2, and 2.4, corresponding to a ± 20% range around the reference value. For each n, the saddle-node bifurcation value ρ_c, the presence or absence of bistability at $\rho = 2.30$, and the corresponding critical dose were recalculated.

3. Results and discussion

3.1. The fixed-parameter model exhibits bistability

The structure of the model analyzed in this section is shown in Figure 1. Each activating interaction displayed in the diagram corresponds to a specific term in Eqs. (1)–(7). The subsequent analysis addresses the dynamical consequences of this structure: the conditions for existence of the persistent attractor (Figure 2), the dependence of long-term outcome on the initial LPS dose (Figure 3), trajectory projections and the relative positions of the equilibria in phase space (Figure 4), and the dependence of the critical switching dose on damage-dependent feedback strength (Figure 5).

Table 2. Equilibria and local stability for the reference parameter set ($\rho = 2.30$, $n = 2$). In all equilibria, $L^* = 0$.

State	C^*	M^*	D^*	Jacobian eigenvalues, day^{-1}	Type
E_0	0	0	0	−1.0000; −0.8000; −0.3800; −0.0600	Stable node
E_1	0.03748	0.06663	0.03831	−1.0000; −0.9442; −0.3636; +0.04075	Saddle
E_2	0.31620	0.56213	0.32323	−1.0619; −1.0000; −0.6208; −0.04514	Stable node

For the reference parameter set, three equilibria were identified within the biologically admissible region. The resolution state E_0 was locally asymptotically stable. The low-amplitude nonzero state E_1 was a saddle with one positive eigenvalue, whereas the higher-amplitude state E_2 was locally

asymptotically stable (Table 2). Thus, the same fixed dynamical system contains two alternative stable long-term outcomes: complete resolution and persistent central inflammatory activity.

One-parameter bifurcation analysis with respect to the damage-dependent feedback coefficient ρ showed that two positive equilibria emerged through a saddle-node bifurcation at $\rho_c = 1.4761$ (Figure 2). For $\rho < \rho_c$, E_0 was the only biologically admissible equilibrium identified and remained locally asymptotically stable; in the numerical simulations performed, trajectories returned to E_0 after the transient input had decayed. For $\rho > \rho_c$, E_0 remained stable, while the saddle equilibrium E_1 and stable persistent equilibrium E_2 coexisted with it. Thus, the key qualitative change is not a loss of stability of E_0, but the emergence of an alternative stable persistent attractor.

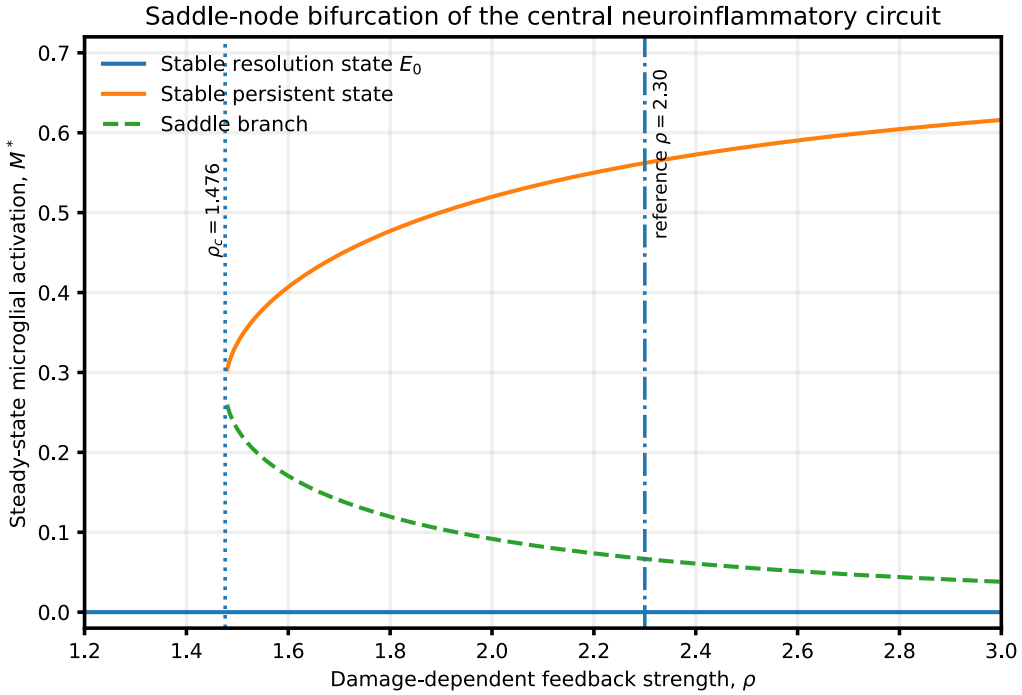


Figure 2. Saddle-node bifurcation of the model with respect to damage-dependent feedback strength ρ. The resolution state E_0 remains stable. At $\rho_c = 1.4761$, a saddle and a stable persistent state emerge. The reference value $\rho = 2.30$ lies within the bistable regime.

3.2. LPS dose determines the long-term outcome in a system with coexisting attractors

No model parameter varies with the LPS dose; dose enters only through $L(0)$. Nevertheless, the simulations produced qualitatively distinct outcomes because the corresponding initial conditions belong to different basins of attraction. For the calibrated reference parameter set, the numerical switching threshold was $D_c = 0.8597$ mg/kg. Doses below this value ultimately returned the system to E_0, whereas doses above it led to convergence to E_2.

A low dose of 0.3 mg/kg produced a small transient increase in C and M, followed by complete resolution. The 0.8 mg/kg dose remained below the switching threshold but produced a prolonged near-boundary trajectory: despite its eventual convergence to E_0, M remained at approximately 0.026 at day 60. In contrast, at 1 mg/kg the corresponding initial condition lay in the basin of E_2 and the

trajectory converged to the persistent state. At 5 mg/kg, the same attractor was reached substantially faster. Thus, increasing the dose does not create a new equilibrium; rather, it determines on which side of the basin boundary the corresponding initial condition lies. This qualitative ordering is consistent with experimental evidence of dose-dependent cytokine and microglial responses in the brain following peripheral LPS exposure [21,22].

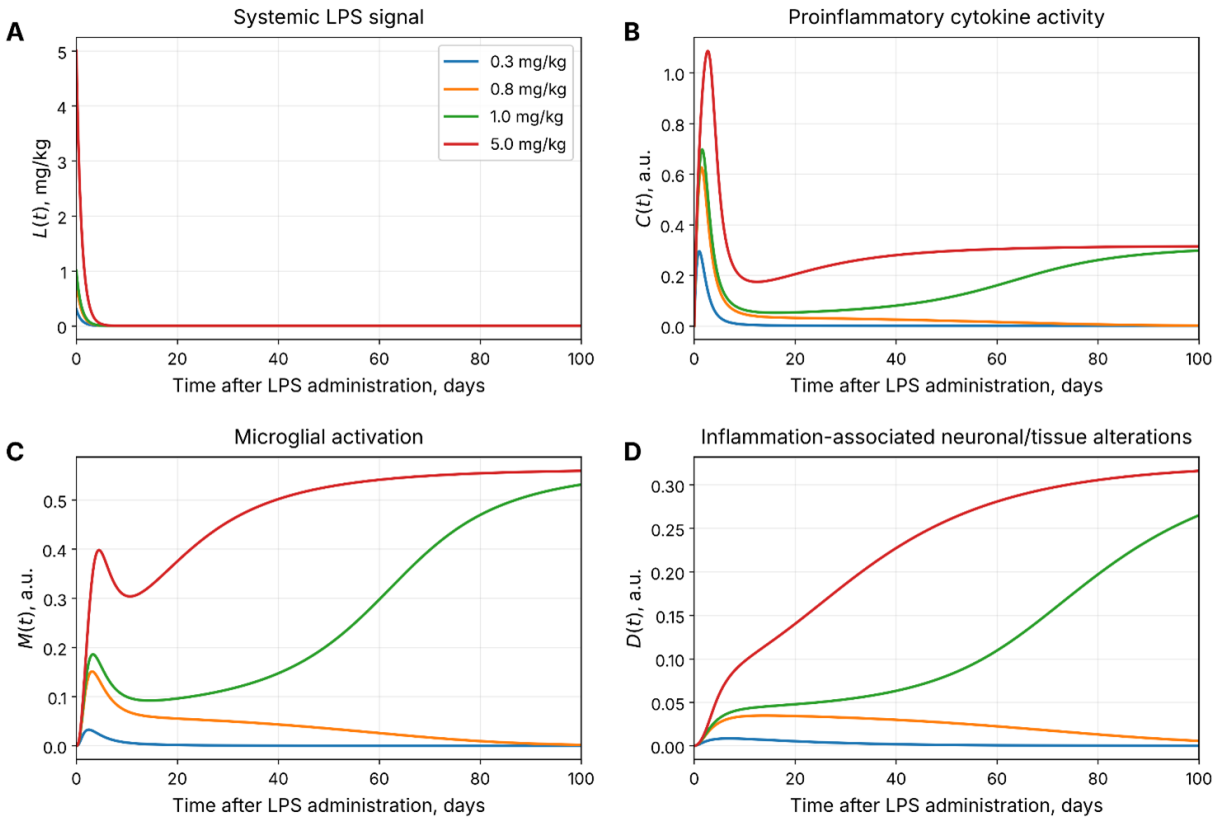


Figure 3. Time evolution of the fixed-parameter model following a single LPS challenge at 0.3, 0.8, 1.0, and 5.0 mg/kg. (A) systemic LPS signal $L(t)$; (B) central cytokine activity $C(t)$; (C) microglial activation $M(t)$; and (D) inflammation-associated neuronal and tissue alterations $D(t)$. The 0.8 mg/kg trajectory is subthreshold and exhibits a prolonged transient followed by resolution, whereas the 1.0 and 5.0 mg/kg trajectories converge to the same persistent attractor at different rates. The numerically determined switching threshold for the reference parameter set is $D_c = 0.8597$ mg/kg.

For the 1 mg/kg trajectory, $C(t)$ reached an acute maximum of approximately 0.70 a.u. at 1.6 days, decreased to approximately 0.052 a.u. around day 16, and subsequently increased again as the central feedback circuit became dominant. At day 60, $C = 0.160$, $M = 0.297$, and $D = 0.109$, whereas the persistent equilibrium values were $C^* = 0.316$, $M^* = 0.562$, and $D^* = 0.323$. Thus, the state at day 60 represents continued convergence toward the persistent attractor rather than residual monotonic decay of the initial acute response.

3.3. Near-threshold slowing as a dynamical interpretation of prolonged responses

The saddle E_1 provides a dynamical interpretation of the prolonged intermediate response within the model. Subthreshold trajectories sufficiently far from the basin boundary return to E_0 without pronounced residence near the saddle. As the initial LPS dose approaches D_c from below, trajectories pass increasingly close to the saddle and remain in its vicinity for longer, thereby prolonging the return to E_0. This produces a prolonged low-amplitude inflammatory transient without any dose-dependent changes in clearance, microglial sensitivity, or damage-related coefficients. In this sense, a prolonged near-threshold inflammatory response may arise from dynamics near the separatrix. This behavior should not be interpreted as mechanistic microglial priming because such an interpretation would require explicit representation of altered responsiveness to a subsequent challenge [23].

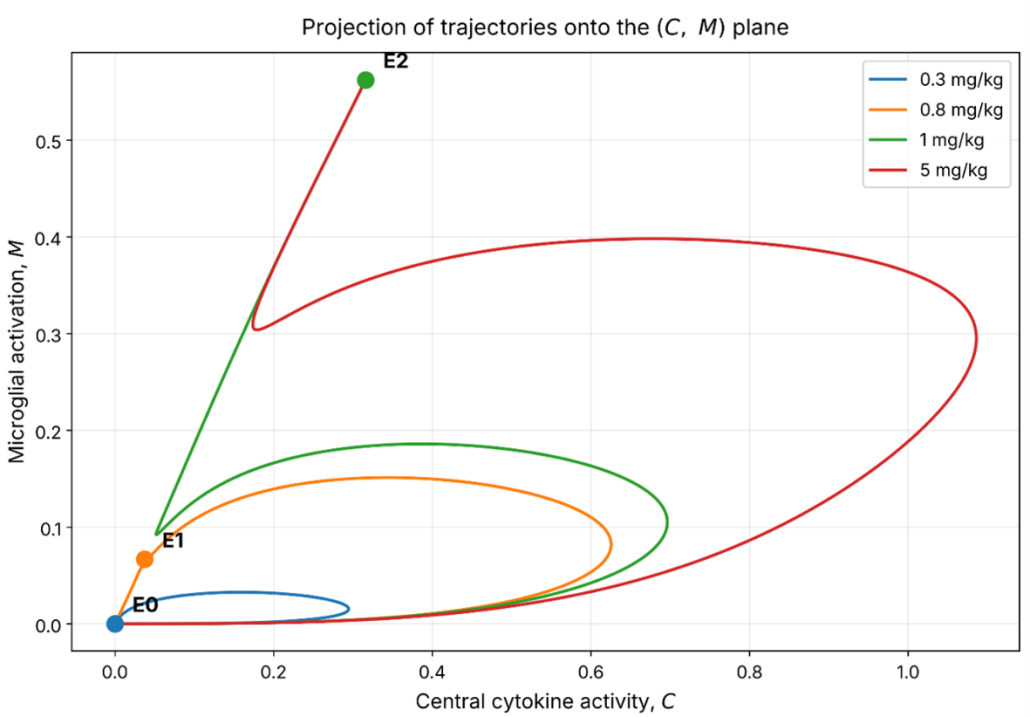


Figure 4. Projections of trajectories of the full four-dimensional system onto the (C, M) plane at different LPS doses. The equilibria E_0 and E_2 are locally asymptotically stable, whereas E_1 is a saddle. Subthreshold trajectories return to E_0, whereas suprathreshold trajectories asymptotically converge to E_2. The three-dimensional stable manifold of the saddle, which separates the basins of attraction in the four-dimensional phase space, is not shown as a curve in this two-dimensional projection.

3.4. Feedback strength determines the existence of the persistent attractor

With all other parameters fixed, the existence of a persistent attractor depends on the magnitude of the damage-dependent feedback coefficient ρ. For $\rho < \rho_c$, where $\rho_c = 1.4761$, no nonzero equilibria exist: increasing the LPS dose increases the amplitude of the transient response, but after the LPS signal has decayed, the system returns to E_0. For $\rho > \rho_c$, a saddle equilibrium E_1 and a stable persistent

equilibrium E_2 emerge. When the critical dose D_c is exceeded, the corresponding initial condition belongs to the basin of E_2 and the corresponding trajectory converges to that state. As ρ increases, D_c decreases (Figure 5). At $\rho = 2.30$, the model gives $D_c \approx 0.86$ mg/kg. As $\rho \to \rho_c{}^{+}$, D_c increases and, close to the bifurcation point, exceeds the upper limit of 6 mg/kg shown in the figure.

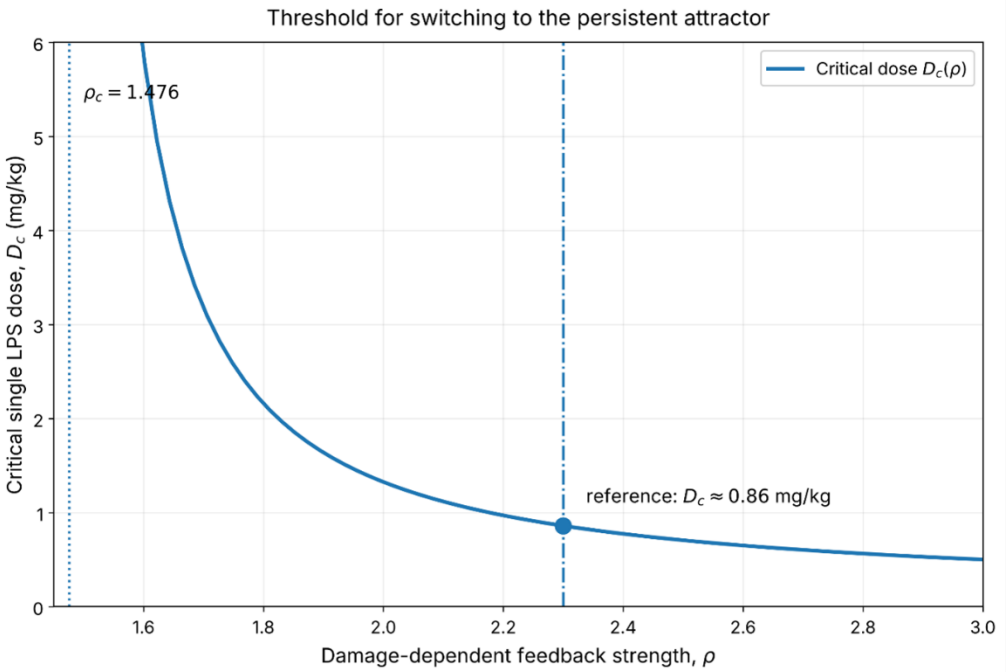


Figure 5. Dependence of the critical single LPS dose D_c on damage-dependent feedback strength ρ. Below the saddle-node bifurcation value ρ_c, the persistent attractor is absent. Above ρ_c, stronger feedback reduces the critical LPS dose at which the line of initial conditions intersects the basin boundary.

3.5. Robustness and sensitivity

Bistability was preserved in 949 of the 1000 Latin hypercube parameter sets (94.9%) generated by simultaneously varying 14 rate, coupling, and half-saturation parameters by ± 20%. The critical dose D_c was determined in 940 of the 949 bistable parameter sets. In the remaining nine sets, D_c could not be identified within the investigated dose range up to 80 mg/kg: the persistent attractor existed mathematically, but LPS-only initial conditions corresponding to doses up to 80 mg/kg did not lie within its basin of attraction. Among the 940 parameter sets with a defined D_c, the median was 0.753 mg/kg, with an interquartile range of 0.486–1.622 mg/kg. The level of microglial activation at the persistent equilibrium was comparatively robust across the 949 bistable parameter sets (median $M^* = 0.569$; interquartile range 0.508–0.614).

The strongest associations between parameters and D_c, as assessed by PRCC, were observed for the microglial activation half-saturation constant K_M (PRCC = +0.945), damage-dependent feedback strength ρ (−0.872), the half-saturation constant of damage-dependent activation K_D (+0.850), the microglial activation rate k_{in} (−0.832), cytokine clearance δ_C (+0.825), and microglial deactivation k_{out} (+0.821) (Supplementary Figure S1). The signs of the coefficients have a direct dynamical

interpretation within the model: stronger positive feedback or faster microglial activation was associated with a lower dose required for switching, whereas a higher activation threshold, weaker damage coupling, faster cytokine clearance, or faster microglial deactivation was associated with a higher switching threshold and a greater tendency toward return to E_0.

Because the PRCC analysis indicated that parameters amplifying the positive feedback lower the switching threshold, the effect of microglia-dependent cytokine production was examined directly. One-parameter continuation in β_C at the reference value $\rho = 2.30$ showed that stronger cytokine production lowers the threshold monotonically, with $D_c = 1.02$, 0.86, 0.75, and 0.47 mg/kg at $\beta_C = 0.36$, 0.45, 0.54, and 1.00 day^{-1}, respectively, while the persistent equilibrium increased from $M^* = 0.545$ to 0.623. Two-parameter continuation of the saddle-node bifurcation in the (ρ, β_C) plane yielded a monotone bistability boundary extending from (ρ, β_C) = (0, 2.03) through (1.476, 0.45), the reference value of β_C, to (2.11, 0), with the reference parameter set (2.30, 0.45) located within the bistable region (Supplementary Figure S3). The absence of positive equilibria at $\rho = 0$ is therefore a property of the reference parameter set rather than a structural feature of the model: the existence of the persistent attractor is determined by the total gain of the positive feedback around the microglia–cytokine–damage loop, to which both ρ and β_C contribute, and the reference parameterization lies in a regime in which damage-dependent feedback is the dominant contributor.

A separate sensitivity analysis of the Hill coefficient showed that bistability was preserved throughout the investigated range $n = 1.6$–2.4 and therefore did not depend on the specific choice $n = 2$. At the same time, the condition $n > 1$ is necessary for the mechanism considered here: only for $n > 1$ is $H'(0) = 0$, which ensures local stability of the resolution state throughout the admissible parameter domain and allows the nonzero states to emerge as a pair through a saddle-node bifurcation. With all other parameters fixed and $\rho = 2.30$, bistability persisted throughout the investigated range $n = 1.6$–2.4. However, the numerical critical dose was sensitive to n, increasing from approximately 0.22 mg/kg at $n = 1.6$ to 3.17 mg/kg at $n = 2.4$ (Supplementary Table S1; Supplementary Figure S2). Thus, $n = 2$ should be regarded as a phenomenological structural assumption.

The linear form of the production terms in Eqs. (2) and (4) was examined separately by replacing them with slope-matched saturating functions: the saddle-node structure and the bistability were retained, with ρ_c and D_c shifted to higher values as saturation was strengthened (Supplementary Table S2, Supplementary Figure S4).

Overall, bistability is a more robust qualitative property of the model than the location and reachability of the switching threshold. The calibrated value $D_c \approx 0.86$ mg/kg should therefore be regarded as a property of the reference parameter set rather than as a universal biological threshold.

3.6. Comparison with published experimental observations

Because C, M, and D are phenomenological variables expressed in arbitrary units, direct comparison of their numerical amplitudes with measured cytokine concentrations, IBA1 expression, or neuronal counts would be inappropriate. In addition, the model resolution state is defined by $C = M = D = 0$, so fold change relative to the model baseline is mathematically undefined. Model assessment was therefore limited to qualitative and temporal correspondence with published experimental observations. A systemic LPS dose of 0.3 mg/kg has been reported to induce an acute increase in brain IL-1β and IL-6 [24], which is consistent with the transient central cytokine response produced by the model at a low dose. A single systemic dose of 1 mg/kg has been associated with prolonged signs of

neuroinflammation in rodents [20]; dose-dependent, transient, and region-specific increases in the microglial population have also been described following systemic LPS administration [25]. This dose range was used in calibrating the location of the model switching threshold. At 5 mg/kg, prolonged changes in brain inflammatory mediators have been reported [26], whereas chronic microglial activation and delayed neurodegeneration have been reported in individual experimental paradigms [2], consistent with the rapid convergence of the model toward the persistent attractor. These comparisons support qualitative and temporal external correspondence but do not constitute quantitative parameter identification. The persistent equilibrium E_2 should be interpreted as a maintained neuroinflammatory state rather than as progressive neurodegeneration itself. Such a state may provide conditions that facilitate subsequent progression of neuronal alterations. Capturing the accumulation of irreversible damage over time would require an additional state variable. The qualitative and temporal correspondence between model regimes and experimental observations is summarized in Table 3.

Table 3. Qualitative and temporal external correspondence between model regimes and experimental observations cited in the present manuscript. Direct fold-change comparison was not performed because the model variables are aggregated quantities expressed in arbitrary units and the baseline level of the resolution state is zero.

LPS dose	Published observation	Model behavior	Role in model assessment
0.3 mg/kg	Acute central cytokine response following systemic LPS administration [24]	Transient increase in C/M followed by resolution	Qualitative external correspondence
1.0 mg/kg	Prolonged signs of neuroinflammation [20]; dose-dependent transient increase in the microglial population [25]	Trajectory on the persistent side of the switching threshold with slow convergence toward E_2	Partially used for threshold calibration; not an independent validation
5.0 mg/kg	Prolonged changes in brain inflammatory mediators [26]; chronic microglial activation and delayed neurodegenerative alterations [2]	Rapid convergence to the persistent attractor	Qualitative external correspondence

Within the model, a nonzero D^* should be interpreted as a dynamically maintained, potentially compensable tissue alteration rather than as irreversible neuronal loss. Systemic LPS exposure has been associated with changes in synaptic or neuronal markers [17,27], whereas more pronounced inflammatory paradigms may be accompanied by overt tissue damage or neurodegenerative alterations [2,28]. The model does not attempt to map $D(t)$ directly onto any single histological or molecular measure.

3.7. Scientific and applied significance

In a fixed-parameter system, the attractors and their stability are properties of the architecture of the central feedback circuit itself, whereas the LPS dose acts only as a transient perturbation that

determines the long-term outcome relative to the existing basins of attraction. Persistence therefore arises from the nonlinear dynamics of the model rather than from dose-dependent changes in kinetic or feedback parameters.

The saddle and its stable manifold also provide a conceptual interpretation of a window of reversibility. Numerical intervention simulations were not performed in the present study. However, the geometry of the basins of attraction supports a testable hypothesis: the ability of a transient intervention to alter the long-term outcome should depend on the current position of the system relative to the basin boundary and on the magnitude of the perturbation induced by the intervention. An intervention capable of moving the state across the stable manifold of the saddle into the basin of E_0 may lead to resolution; as the trajectory moves farther from the basin boundary, a stronger perturbation may be required to produce such a transition. This is a model-based hypothesis rather than a demonstrated therapeutic effect, but it provides a testable rationale for investigating the timing and magnitude of interventions in preclinical experiments. A sustained reduction of ρ below the saddle-node bifurcation point eliminates the persistent equilibrium for as long as that parameter regime is maintained.

The model may therefore serve as a hypothesis-generating tool for experimental design by distinguishing changes that affect the magnitude of the acute response from changes that modify the underlying feedback architecture and thereby alter the existence or reachability of persistent states. However, the present parameterization is preclinical and phenomenological and should not be directly extrapolated to human disease or clinical dosing.

3.8. Model limitations and future directions

The proposed model is phenomenological and is intended to analyze qualitative dynamical regimes rather than reproduce the kinetics of individual molecular markers. First, signal transmission from the systemic to the central level is coarse-grained: peripheral cytokine dynamics, endothelial signaling, immune-cell migration, and BBB permeability are not represented as separate state variables. Their combined initiating contribution is represented by the effective transient input $\sigma_L(L)$. Thus, the model describes the dynamics of a central neuroinflammatory circuit following systemic stimulation rather than the mechanistic details of peripheral-to-CNS signal transmission.

Second, C, M, and D are aggregated variables and do not correspond directly to concentrations of individual cytokines, numbers of activated microglial cells, or quantitative measures of neuronal death. The variable $D(t)$ should be interpreted as the aggregate severity of inflammation-associated neuronal and tissue alterations. Because Eq. (4) contains the resolution term $k_{D,\mathrm{out}}D$, D may decrease as inflammatory drive subsides through processes of repair and compensation. Accordingly, a nonzero D^* at the persistent equilibrium represents a dynamically maintained pathological tissue state in which ongoing cytokine- and microglia-dependent generation of alterations is balanced by resolution or compensation. Phenomenologically, this may include cellular stress, synaptic alterations, reactive tissue remodeling, and other persistent damage-associated changes. D^* should not be interpreted as the number or fraction of dead neurons. Accordingly, the model is compared with experimental data qualitatively and in terms of temporal behavior rather than through direct quantitative correspondence to specific markers.

Third, the reference parameter set was calibrated computationally. In particular, ρ was selected so that a dose of 1 mg/kg lay on the persistent side of the reference switching threshold; therefore, D_c is

a calibration-dependent quantity. Sensitivity analysis further showed that the numerical value of D_c depends substantially on parameterization, including the Hill coefficient n, despite the comparative robustness of bistability itself.

Fourth, the model includes only proinflammatory and damage-dependent feedback and does not explicitly represent active anti-inflammatory mechanisms, such as IL-10 signaling and specialized pro-resolving mediators. The net effect of processes contributing to attenuation and resolution of the inflammatory response is captured phenomenologically by the linear clearance, deactivation, and resolution terms ($-\delta_C \cdot C$, $-k_{out} \cdot M$, and $-k_{D,out} \cdot D$). Future extensions could include an additional state variable $A(t)$ representing anti-inflammatory activity, with inhibitory effects on proinflammatory cytokine activity and/or microglial activation. Models of the acute inflammatory response that incorporate an explicit anti-inflammatory mediator provide a template for such an extension [3].

Fifth, the model includes only proinflammatory and damage-dependent feedback and does not explicitly represent anti-inflammatory cytokines, microglial phenotypic heterogeneity, astrocytes, adaptive immune responses, repeated LPS challenges, age- or sex-related effects, or therapeutic intervention. These factors may substantially influence the response to LPS [19]. The model also assumes the absence of prior inflammatory exposure. Under real biological conditions, previous infections, systemic inflammatory episodes, and repeated exposure to LPS may alter the sensitivity of the neuroinflammatory circuit through priming or tolerance and thereby shift the switching threshold D_c.

Future extensions of the model could examine interventions that modify parameters of the neuroinflammatory circuit and thereby alter the switching threshold. In particular, a preventive intervention that weakens positive feedback or strengthens resolution processes could theoretically increase D_c and reduce the likelihood of transition to the persistent state. Finally, the model was formulated for LPS paradigms in rodents and is not intended for direct extrapolation to human systemic inflammation or clinical dosing without additional experimental parameterization and validation.

4. Conclusions

We developed a fixed-parameter ODE model of a central neuroinflammatory circuit to investigate how a transient systemic LPS challenge can lead to distinct long-term outcomes. With sufficiently strong damage-dependent feedback, the model exhibits bistability between a stable resolution state and a stable persistent neuroinflammatory state, together with a coexisting saddle equilibrium. The LPS dose changes only the magnitude of the transient initial perturbation and determines which of the coexisting attractors the corresponding trajectory converges to. Near the basin boundary, prolonged inflammatory transients arise naturally from slow dynamics in the vicinity of the saddle, whereas higher suprathreshold doses approach the persistent attractor more rapidly. The bistable structure is preserved under broad parameter variation and moderate variation of the Hill coefficient, although the numerical critical dose is parameter-sensitive and should be interpreted as a calibrated rather than universal quantity. The proposed framework therefore provides a dynamical-systems interpretation of resolution, prolonged near-threshold responses, and persistent neuroinflammatory activity without introducing dose-dependent changes in model parameters.

Use of generative-AI tools declaration

The authors used the Assistive-AI tools Grammarly and Curie for grammar checking, language polishing, and improvement of clarity and readability. These tools were used solely for editorial assistance and did not contribute to the generation of scientific ideas. No Generative-AI tools were used in the creation of this article. All suggested changes were carefully reviewed and edited by the authors, who take full responsibility for the accuracy, originality, and integrity of the manuscript.

Conflict of interest

The authors declare no conflicts of interest.

Author contributions

The study concept and design were jointly developed by all authors. EK and DT performed the study and analyses. EK and EL prepared the original draft of the manuscript. MK supervised the project and contributed to manuscript review and editing. All authors reviewed and approved the final version.

Data availability

The numerical results presented in this study were generated using Python 3.12, SciPy 1.16, and Matplotlib 3.10. The source code required to reproduce the model equations, equilibria, bifurcation point, critical-dose analysis, and sensitivity analyses is available from the corresponding author upon reasonable request.

References

1. Skelly DT, Hennessy E, Dansereau MA, et al. (2013) A systematic analysis of the peripheral and CNS effects of systemic LPS, IL-1β, TNF-α and IL-6 challenges in C57BL/6 mice. *Plos One* 8: e69123. https://doi.org/10.1371/journal.pone.0069123
2. Qin L, Wu X, Block ML, et al. (2007) Systemic LPS causes chronic neuroinflammation and progressive neurodegeneration. *Glia* 55: 453–462. https://doi.org/10.1002/glia.20467
3. Reynolds A, Rubin J, Clermont G, et al. (2006) A reduced mathematical model of the acute inflammatory response: I. Derivation of model and analysis of anti-inflammation. *J Theor Biol* 242: 220–236. https://doi.org/10.1016/j.jtbi.2006.02.016
4. Vaughan LE, Ranganathan PR, Kumar RG, et al. (2018) A mathematical model of neuroinflammation in severe clinical traumatic brain injury. *J Neuroinflamm* 15: 345. https://doi.org/10.1186/s12974-018-1384-1
5. Colonna M, Butovsky O (2017) Microglia function in the central nervous system during health and neurodegeneration. *Annu Rev Immunol* 35: 441–468. https://doi.org/10.1146/annurev-immunol-051116-052358
6. Ransohoff RM, Perry VH (2009) Microglial physiology: unique stimuli, specialized responses. *Annu Rev Immunol* 27: 119–145. https://doi.org/10.1146/annurev.immunol.021908.132528

7. Hoogland IC, Houbolt C, van Westerloo DJ, et al. (2015) Systemic inflammation and microglial activation: systematic review of animal experiments. *J Neuroinflamm* 12: 114. https://doi.org/10.1186/s12974-015-0332-6
8. Sun Y, Koyama Y, Shimada S (2022) Inflammation from peripheral organs to the brain: how does systemic inflammation cause neuroinflammation? *Front Aging Neurosci* 14: 903455. https://doi.org/10.3389/fnagi.2022.903455
9. Peng X, Luo Z, He S, et al. (2021) Blood-brain barrier disruption by lipopolysaccharide and sepsis-associated encephalopathy. *Front Cell Infect Microbiol* 11: 768108. https://doi.org/10.3389/fcimb.2021.768108
10. Zhao J, Bi W, Xiao S, et al. (2019) Neuroinflammation induced by lipopolysaccharide causes cognitive impairment in mice. *Sci Rep* 9: 5790. https://doi.org/10.1038/s41598-019-42286-8
11. Kim HJ, Kim H, Lee JH, et al. (2023) Toll-like receptor 4 (TLR4): new insight immune and aging. *Immun Ageing* 20: 67. https://doi.org/10.1186/s12979-023-00383-3
12. Nürnberger F, Ott D, Claßen R, et al. (2022) Systemic lipopolysaccharide challenge induces inflammatory changes in rat dorsal root ganglia: an ex vivo study. *Int J Mol Sci* 23: 13124. https://doi.org/10.3390/ijms232113124
13. Gao HM, Zhou H, Zhang F, et al. (2011) HMGB1 acts on microglia Mac1 to mediate chronic neuroinflammation that drives progressive neurodegeneration. *J Neurosci* 31: 1081–1092. https://doi.org/10.1523/JNEUROSCI.3732-10.2011
14. Zhou R, Chen SH, Zhao Z, et al. (2023) Complement C3 enhances LPS-elicited neuroinflammation and neurodegeneration via the Mac1/NOX2 pathway. *Mol Neurobiol* 60: 5167–5183. https://doi.org/10.1007/s12035-023-03393-w
15. Suleiman Khoury Z, Sohail F, Wang J, et al. (2024) Neuroinflammation: a critical factor in neurodegenerative disorders. *Cureus* 16: e62310. https://doi.org/10.7759/cureus.62310
16. Jang J, Hong A, Chung Y, et al. (2022) Interleukin-4 aggravates LPS-induced striatal neurodegeneration in vivo via oxidative stress and polarization of microglia/macrophages. *Int J Mol Sci* 23: 571. https://doi.org/10.3390/ijms23010571
17. Jung H, Lee D, You H, et al. (2023) LPS induces microglial activation and GABAergic synaptic deficits in the hippocampus accompanied by prolonged cognitive impairment. *Sci Rep* 13: 6547. https://doi.org/10.1038/s41598-023-32798-9
18. Batulin D, Lagzi F, Vezzani A, et al. (2022) A mathematical model of neuroimmune interactions in epileptogenesis for discovering treatment strategies. *iScience* 25: 104343. https://doi.org/10.1016/j.isci.2022.104343
19. da Silva AAF, Fiadeiro MB, Bernardino LI, et al. (2024) Lipopolysaccharide-induced animal models for neuroinflammation: an overview. *J Neuroimmunol* 387: 578273. https://doi.org/10.1016/j.jneuroim.2023.578273
20. Maystrenko V, Ivleva I, Krytskaya D, et al. (2021) Changes in activity of μ- and m-calpains and signs of neuroinflammation in the hippocampus and striatum of rats after single intraperitoneal injection of subseptic dose of endotoxin. *Metab Brain Dis* 36: 1917–1928. https://doi.org/10.1007/s11011-021-00755-y
21. Quan N, Stern EL, Whiteside MB, et al. (1999) Induction of pro-inflammatory cytokine mRNAs in the brain after peripheral injection of subseptic doses of lipopolysaccharide in the rat. *J Neuroimmunol* 93: 72–80. https://doi.org/10.1016/S0165-5728(98)00193-3

22. Brandi E, Torres-Garcia L, Svanbergsson A, et al. (2022) Brain region-specific microglial and astrocytic activation in response to systemic lipopolysaccharides exposure. *Front Aging Neurosci* 14: 910988. https://doi.org/10.3389/fnagi.2022.910988
23. Lima M N, Barbosa-Silva M C, Maron-Gutierrez T (2022) Microglial priming in infections and its risk to neurodegenerative diseases. *Front Cell Neurosci* 16: 878987. https://doi.org/10.3389/fncel.2022.878987
24. Pamplona F A, Vitória G, Sudo F K, et al. (2022) Age-linked suppression of lipoxin A4 associates with cognitive deficits in mice and humans. *Transl Psychiatry* 12: 439. https://doi.org/10.1038/s41398-022-02208-1
25. Furube E, Kawai S, Inagaki H, et al. (2018) Brain region-dependent heterogeneity and dose-dependent difference in transient microglia population increase during lipopolysaccharide-induced inflammation. *Sci Rep* 8: 2203. https://doi.org/10.1038/s41598-018-20643-3
26. Bossù P, Cutuli D, Palladino I, et al. (2012) A single intraperitoneal injection of endotoxin in rats induces long-lasting modifications in behavior and brain protein levels of TNF-α and IL-18. *J Neuroinflamm* 9: 101. https://doi.org/10.1186/1742-2094-9-101
27. Rezaei S, Banasr M, Prevot TD, et al. (2025) Brain-derived neurotrophic factor prevents LPS-induced dysregulation of GABAergic interneuron markers in mouse hippocampus. *Front Cell Neurosci* 19: 1675003. https://doi.org/10.3389/fncel.2025.1675003
28. He Q, Qi Q, Ibeanu GC, et al. (2024) B355252 suppresses LPS-induced neuroinflammation in the mouse brain. *Brain Sci* 14: 467. https://doi.org/10.3390/brainsci14050467



AIMS Press

© 2026 the Author(s), licensee AIMS Press. This is an open access article distributed under the terms of the Creative Commons Attribution License (http://creativecommons.org/licenses/by/4.0)